Contents lists available at ScienceDirect

Chemical Engineering Research and Design

journal homepage: www.elsevier.com/locate/cherd

CFD simulation of heat transfer in a two-dimensional vertical enclosure

A.A. Ganguli, A.B. Pandit, J.B. Joshi*

Institute of Chemical Technology, University of Mumbai, Matunga, Mumbai 400019, India

ABSTRACT

In order to predict the variation in heat transfer coefficient setup by natural convection, independent CFD simulations have been performed for various tall slender vertical geometries (100 mm < H < 1000 mm) with varying gap widths (5 mm < L < 84.7 mm) and temperature differences (5 K < ΔT < 90 K) covering the ranges reported in the literature (Batchelor, G.K., 1954. Heat transfer by free convection across a closed cavity between vertical boundaries at different temperatures. Quart. Appl. Math., 12, 209–233; Newell, M.E., Schmidt, F.W., 1970. Heat transfer by laminar natural convection within rectangular enclosures. Trans. ASME C: J. Heat Transf., 92, 159–167; Yin, S.H., Wung, T.Y., Chen, K., 1978. Natural Convection in an air layer enclosed within rectangular cavities. Int. J. Heat Mass Transf., 21, 307–315; Elsherbiny, S.M., Raithby, G.D., Hollands K.G.T., 1982. Heat transfer by natural convection across vertical and inclined air layers. Trans. ASME J. Heat Transf., 104: 96–102; Lee, Y., Korpela, S., 1983. Multicellular natural convection in a vertical slot. J. Fluid Mech., 126, 91–124) and compared with their own experimental and numerical studies. A good agreement of Nusselt number (±10%) has been found between the CFD predictions and the literature data. Further, simulations were carried out for gap widths (5 mm ≤ L ≤ 25 mm), heights (100 mm ≤ H ≤ 1000 mm) (4 ≤ AR ≤ 200) and temperature differences (20 K ≤ ΔT ≤ 90 K, 5.99E + 02 ≤ Ra ≤ 3.15E + 05) and a correlation for the estimation of Nu has been proposed. The sensitivity analysis shows %deviation of heat transfer coefficient only in the range of ±10%. A generalized correlation based on all the above results encompassing the effect of height, gap width and temperature difference has also been proposed, which can be used to accurately estimate heat losses from a vertical air gap acting as an insulation.

Keywords: Natural convection; Rectangular slots; Correlation; Flow patterns; Heat Transfer; CFD simulation

1. Introduction

1.1. Insulation in double pane windows

Energy conservation and savings has been one of the prime concerns of energy researchers. One such interesting application of energy conservation is that of double pane windows. The energy efficient windows should possess some important characteristics like low heat loss, practically no or less air leakage and warmer window surfaces to minimize condensation. Some of the important energy features of these windows are shown in Fig. 1, namely, multiple layers of glazing, thickness of air space, low-conductivity gas fill, tinted glass coatings, low emissive-coatings and edge spacers. An optimum window design and glazing specification can reduce energy consumption for air-conditioning considerably (10–50%) in most climates. In commercial, industrial and institutional buildings, an optimum window design has the potential to reduce lighting and heating, ventilation and air-conditioning (HVAC) costs by 10–40%. The present problem is an example of natural convection as an internal bound flow in which interaction takes place between a finite amount of fluid and the walls enclosing them. A design engineer is interested in understanding the complexity of the flow inside and its effect on the heat transfer. The complexity of the problem does not allow analytical solutions, so one has to rely on experiments and numerical simulations.

* *Corresponding author*. Tel.: +91 22 2414 5616; fax: +91 22 2414 5614.
E-mail address: abp@udct.org (A.B. Pandit).
Received 25 May 2008; Received in revised form 21 October 2008; Accepted 6 November 2008
0263-8762/$ – see front matter © 2008 The Institution of Chemical Engineers. Published by Elsevier B.V. All rights reserved.
doi:10.1016/j.cherd.2008.11.005

Nomenclature

AR	aspect ratio (H/L)
C_p	specific heat of the fluid ($J\,kg^{-1}\,K^{-1}$)
g	acceleration due to gravity ($m\,s^{-2}$)
Gr_L	Grashof number based on gap width ($g\beta\,\Delta T\,\rho^2L^3/\mu^2$)
h	convective heat transfer coefficient ($W\,m^{-2}\,K^{-1}$)
H	height of the enclosure (m)
k	thermal conductivity ($W\,m^{-1}\,K^{-1}$)
L	gap width of enclosure (m)
Nu	Nusselt number (hL/k)
p	pressure per unit surface ($N\,m^{-2}$)
P	dimensionless pressure ($p/\rho V_0^2$)
Pr	Prandtl number ($C_p\mu/k$)
Ra	Rayleigh number based on gap width ($g\beta\,\Delta T\,L^3/\nu\alpha$)
t	time (s)
t^*	dimensionless time, $t^* = t/t_0$
t_0	initial time (s) $t_0 = L/V_0$
T	temperature (K)
u	horizontal velocity ($m\,s^{-1}$)
U	dimensionless horizontal velocity (u/V_0)
v	vertical velocity ($m\,s^{-1}$)
V	dimensionless vertical velocity (v/V_0)
V_0	initial velocity ($m\,s^{-1}$) ($V_0 = \sqrt{g\beta\,\Delta T\,L}$)
x	co-ordinate in x-direction (m)
X	dimensionless horizontal length (x/L)
y	co-ordinate in y-direction (m)
Y	dimensionless vertical length)y/L)

Greek symbols

α	thermal diffusivity ($m^2\,s^{-1}$)
β	coefficient of thermal expansion (K^{-1})
δ	thermal boundary layer thickness (m)
μ	dynamic viscosity ($kg\,m^{-1}\,s^{-1}$)
ν	kinematic viscosity ($m^2\,s^{-1}$)
ρ	density ($kg\,m^{-3}$)
ϕ	scalar or vector quantity
θ	dimensionless temperature $\theta = (T - T_m)/(T_h - T_c)$
θ'	weighting factor

Subscripts

B	bottom
C	critical as with *Ra*, *Gr*
C	cold wall temperature
f	face cell
H	hot wall
i	direction co-ordinate
j	direction co-ordinate
m	mean
p	pressure
SOU	second-order upwind
t	thermal
T	top

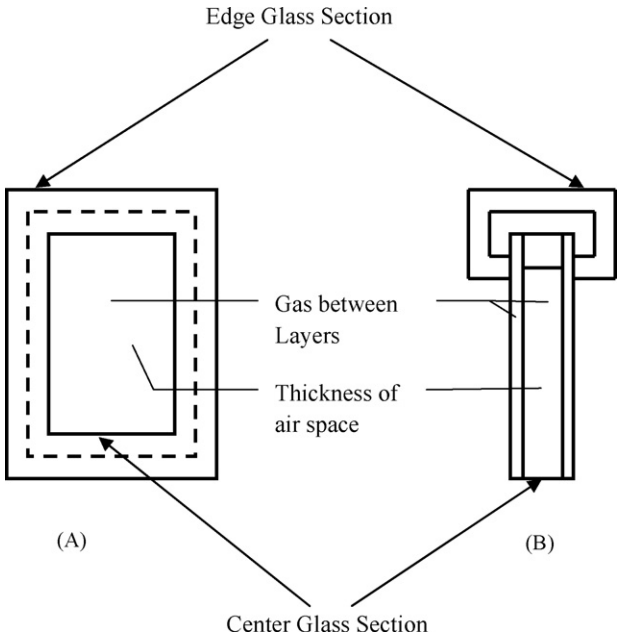

Fig. 1 – Schematic of a typical double pane window: (A) front view and (B) side view.

1.2. *Mechanism of flow and heat transfer in any vertical enclosure heated from one side and cooled from other side*

Fig. 2 shows a typical vertical enclosure with height *H* and gap width *L*. Constant temperature is maintained at the left and right walls such that the right wall is at temperature (T_H), ($320\,K \le T_H \le 410\,K$) and left wall at temperature (T_C) ($T_C = 300\,K$). Initially, the fluid inside the enclosure is kept at a uniform temperature T_m. ($T_m = 300$). Due to the temperature difference arising between the left and right walls, fluid rises along the hot wall, turns at the top end, sinks along the cold wall, and turns again around at the bottom to set up unicellular convection. Three dimensionless parameters describe such a flow namely the Rayleigh number (*Ra*) (ratio of buoyancy to viscous forces) ($g\beta\,\Delta T\,L^3/\nu\alpha$), the Prandtl number, *Pr* ($C_p\mu/k$) (ratio of momentum to thermal diffusivity) and the aspect ratio, AR (*H*/*L*) (height to gap width ratio) of the geometry under consideration. The flows are classified into three regimes: the conduction regime, the transition regime and the boundary layer regime. The conduction regime is governed by conduction; the transition regime by conduction near the walls and convection in the core and the boundary layer regime by convection in the core and conduction limited to a relatively thin boundary layer near the wall. The typical temperature profiles of direction of conduction and boundary layer regimes are shown in Fig. 3. Fig. 3A shows a typical vertical enclosure ($AR > 10$) and Fig. 3B shows a typical linear temperature profile expected in the conduction regime ($1000 < Ra < 3500$) and Fig. 3C shows the temperature profile with boundary layers along the side walls. In the convection dominated region (the core) multiple cells are formed under some specific conditions (Ganguli et al., 2007). At low *Ra* numbers ($3000 \le Ra \le 10^4$, depending on the values of AR, $5 \le AR \le 40$ and $Pr = 0.73$) the cells form and remain steady for infinite time. These have been termed as secondary cells. For higher *Ra* numbers ($10^4 \le Ra \le 10^6$ depending on the values of AR, $5 \le AR \le 110$ and $Pr = 0.73$) the cells move and merge and reappear

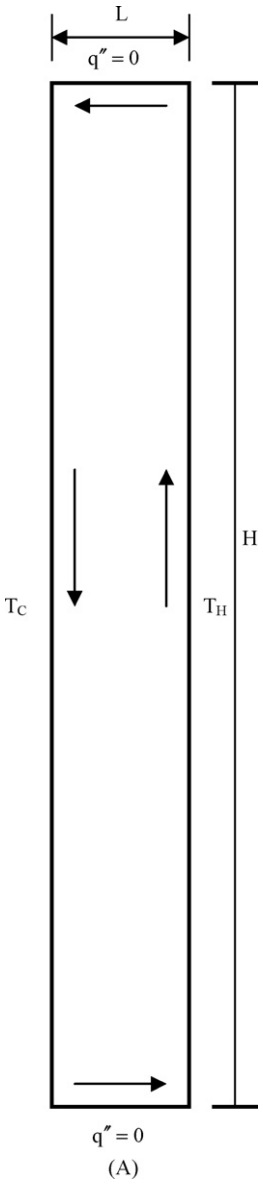

Fig. 2 – Schematic of a rectangular enclosure differentially heated and cooled from both sides.

due to the presence of self generated pressure gradients. During the process of moving and merging, between two secondary cells, small cells are seen which assist in the cell merging process. These are termed as tertiary cells (Elder, 1965).

1.3. *Previous work*

Tables 1A–1C give a summary of the previous analytical, experimental and numerical studies together with their important observations and limitations. The two-dimensional flow and its effect on the heat transfer rates has been investigated for nearly seven decades. These efforts can be classified as: (A) analytical approach (Batchelor, 1954), (B) experimental (Yin et al., 1978; Elsherbiny et al., 1982; Wakitani, 1996) and (C) numerical (Newell and Schmidt, 1970; Korpela et al., 1982; Le Quéré, 1990; Wakitani, 1994; Wakitani, 1997; Zhao et al., 1997; Lartigue et al., 2000). The investigations were carried out mainly with two objectives (a) to develop correlations between the geometry and heat transfer rates (Jakob, 1949; Yin et al., 1978; Elsherbiny et al., 1982) and (b) to understand the effect of convection induced flow patterns on heat transfer (Elder, 1965; Korpela et al., 1982; Le Quéré, 1990; Wakitani, 1994; Wakitani, 1997; Zhao et al., 1997; Lartigue et al., 2000). On the basis of CFD simulations, Newell and Schmidt (1970) first proposed correlations for the estimation of Nusselt number *Nu*, as a function of *Gr* number and AR (Table 1A). The complexity of the flow in the core region with respect to ΔT and AR prompted researchers (Yin et al., 1978; Lee and Korpela, 1983) to investigate *Nu* number predictions with better experimental and numerical techniques, especially with air as a working fluid. Yin et al. (1978) found that the value of *Nu* number was directly proportional to *Gr* number but inversely proportional to AR, though, the dependence on AR was weak (Table 1A). Lee and Korpela (1983) analyzed the critical values of *Ra* number for the onset of multicellular convection and heat transfer just after its formation. Elsherbiny et al. (1982) found a generalized correlation for the prediction of heat transfer coefficients over a wide range *Ra* ($1000 \leq Ra \leq 10^7$) and AR ($10 \leq AR \leq 110$) (Table 1). The authors (Le Quéré, 1990; Wakitani, 1994, 1997; Zhao et al., 1997; Lartigue et al., 2000) observed that the transition of multiple cells did not have any significant effect on the average Nusselt number irrespective of the imposed initial conditions for the solution of the numerical scheme. A significant contribution has been made by Zhao et al. (1997) who numerically investigated the multicellular convection in high AR enclosures ($10 \leq AR \leq 110$) to be able to use it as a tool to more accurately predict heat transfer. This prompted researchers to focus on high AR enclosures, who then directed their efforts to understand the flow patterns and their effect on heat transfer. Lartigue et al. (2000) carried out experimental (PIV) measurements and numerical studies ($AR = 40$, $3 \times 10^3 \leq Ra \leq 2 \times 10^5$) and compared their predicted heat transfer coefficients with

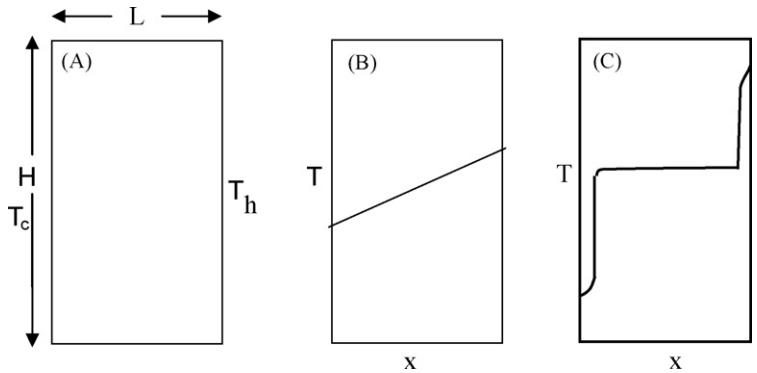

Fig. 3 – Different types of flow regimes: (A) high aspect ratio enclosure; (B) temperature distribution across the high aspect ratio enclosure in the conduction regime; (C) temperature distribution across the high aspect ratio enclosure in the boundary layer regime.

Table 1A – Details of various geometry, range and proposed correlations available in literature.

Author	Fluid	Geometry details (aspect ratio range)	Range of Rayleigh/Grashof number	Proposed correlations and Nusselt numbers
Jakob (1946)	Air	3.12–42.2	$2 \times 10^4 < Gr_L < 2 \times 10^5$	$Nu = 0.18(Gr_L)^{0.25}$ $(AR)^{-0.111}$ $Nu = 0.065(Gr_L)^{0.333}$ $(AR)^{-0.111}$
Batchelor (1954)	Air	–	$10^3 < Ra < 10^7$	–
Eckert and Carlson (1961)	Air	–	$8 \times 10^4 < Gr_L < 2 \times 10^5$	$Nu = 0.119(Gr_L)^{0.3}$ $(AR)^{-0.1}$
Newell and Schmidt (1970)	Air	AR = 1; AR = 5	$4 \times 10^3 < Gr < 1.4 \times 10^6$	$Nu = 0.0547(Gr_L)^{0.3947}$; $Nu = 0.155(Gr_L)^{0.315}$ $(AR)^{-0.265}$
Yin et al. (1978)	Air	4.9 < AR < 78.7	$1500 < Ra < 7 \times 10^6$	$Nu = 0.091 Gr_L{}^{0.307}$ $Nu = 0.21 Gr_L{}^{0.269} AR^{-0.131}$
Elsherbiny et al. (1982)	Air	5 < AR < 110	$1000 < Ra < 10^7$	$Nu_1 = 0.0605 Ra^{1/3}$ $Nu_2 = \left[1 + \left\{0.104 Ra^{0.293}/1 + (6310/Ra)^{1.36}\right\}^3\right]^{1/3}$ $Nu_3 = 0.242(Ra/AR)^{0.272}$ $Nu = [Nu_1, Nu_2, Nu_3]_{max}$
Lee and Korpela (1983)	Air	5 < AR < 60	$9.23 \times 10^2 < Ra < 1.78 \times 10^4$	–
Le Quéré (1990)	Air	AR = 16	$6 \times 10^3 < Ra < 4 \times 10^4$	–
Wakitani (1997)	Air, Glycerine	AR = 16	$9 \times 10^3 < Ra < 3 \times 10^5$	–
Zhao et al. (1997)	Air	10 < AR < 100	$3550 < Ra < 5 \times 10^6$	–
Lartigue et al. (2000)	Air	AR = 40	$3550 < Ra < 2 \times 10^4$	–

Table 1B – Details of experimental techniques used by different researchers.

Author	Experimental technique				
	Measurement	Equipment for measurement	Accuracy	Range of *Ra*, *Gr* and AR	[a]Limitations
Yin et al. (1978)	Measurement of heat flux	Thermocouples	Accurate temperature measurements with 20 strip electrical heaters. Mica sheet with Nichrome ribbon wound around. Aluminium plate was used for hot plate while copper was used for cold plates	$1500 < Ra < 7 \times 10^6$, $1000 < Ra < 10^7$, $Pr = 0.73$	12
Elsherbiny et al. (1982)	Heat flux measurement to measure heat transfer coefficient	Thermocouples	Error in the heat flux was 075 W m^{-2}. Error in temperature linearity was maintained within 1% at the highest *Ra* number possible. For high AR the width *L* was maintained within an uncertainty of 0.1% with high precision machining. Temperature variations within each plate was within 0.02 K	$5 < AR < 110$, $1000 < Ra < 10^7$, $Pr = 0.73$	15

[a] Limitations with numbers specified after Table 1C.

Table 1C – Solution schemes used by earlier researchers.

Author	Numerical technique					[a]Assumptions	[a]Conclusion	[a]Limitations
	Governing equations	Numerical method	Grid	Scheme	Time-step			
Batchelor (1954)	Stream-Function Vorticity	Analytical solutions	–	–	–	1, 2, 5, 8, 9, 10	1, 7	1, 3, 5,17
Gill (1966)	Boundary layer equations	Analytical solutions	–	–	–	1, 2, 3, 4, 5, 7, 8, 9, 10	1	3, 17
Newell and Schmidt (1970)	Stream-Function Vorticity	Crank–Nicholson method	40×40	Central difference scheme	0.0001	1, 2, 3, 4, 5, 6, 7, 8, 9, 10	4, 5, 6	11, 12
Lee and Korpela (1983)	Navier Stokes equations	FEM, FDM, Galerkin method.	17×129	Arakawa scheme	1×10^{-3} $Ra = 2000$; 2×10^{-4} $Ra = 10^5$	1, 2, 3, 4, 5, 6, 7, 8, 9, 10	6, 7, 10, 11	4, 14
Le Quéré (1990)	Navier Stokes equations	Chebyshev Polynomials	–	Third-order schemes	0.001	1, 2, 3, 4, 5, 6, 7, 8, 9, 10	8, 11, 12	3, 9
Wakitani (1997)	Dimensionless Navier Stokes equations	Euler Implicit Adam–Brashforth	Non-uniform grid 25×121	Third-order upwinding	0.0005	1, 2, 3, 4, 5, 6, 7, 8, 9, 10	14	2, 9,10
Zhao et al. (1997)	Dimensionless Navier Stokes equations	FEM	Non-uniform grid	Upwind scheme	0.0001	1, 2, 3, 4, 5, 6, 7, 8, 9, 10	15	1, 9, 10
Lartigue et al. (2000)	Dimensionless Navier Stokes equations	FVM	Non-uniform grid	Upwind scheme			16	1, 2, 9, 10,11

Assumptions: (1) A different condition on the temperature field at the two horizontal boundaries would only alter the solution significantly in the vicinity of these boundaries. (2) Boussinesq approximation is made, i.e., density differences are only important in producing buoyancy. (3) Properties of the fluid except viscosity do not change significantly in temperature range $T_h < T_m < T_c$. (4) Variation in viscosity is assumed. (5) Heat transfer by radiation is not included. (6) Length of enclosure is sufficiently large for two-dimensional motion to be assumed. (7) Constant properties except in formulation of buoyancy term. (8) Fluid is Newtonian and incompressible. (9) Flow is laminar and two-dimensional. (10) Appropriateness of fairly general but still idealized thermal boundary conditions. **Conclusions:** (1) Flow in a vertical slot ($AR > 5$) remains laminar till a critical Grashof number (Gr) above which it is restricted to the boundary layer. (2) Above $Ra > 1 \times 10^5$ secondary flows (multiple cells) are seen and above $Ra > 1 \times 10^7$ tertiary cells are seen (counter-rotating, moving cells). (3) The possibility that tertiary flows arise from instability of secondary flow. (4) Fine grid gives better predictions of flow patterns. (5) Finite Difference method serves as an important tool for predicting flow patterns for complex geometries with required accuracy. (6) For low Prandtl numbers cells settle down rapidly and no quasiperiodic behavior is obtained. (7) High heat transfer near the bottom of the hot wall and near the top of the cold wall can cause local non-uniformities in wall temperature in these regions. These may be the reason for discrepancy between experiments and theory. (8) Cells increase due to instability with time and after a specific time period reverts back to unicellular pattern. Return to unicellular structure is complex than previously analyzed. (9) Number of cells increase step by step and each change is characterized by hysteresis. (10) Initial condition is very important in the case of numerical simulations. (11) Accurate predictions can be made when numerical simulations are done by gradually increasing the Rayleigh number with second set of simulations taking the initial input from results of first set of simulations. (12) With increase in Rayleigh number different number of cells are formed which may revert back to a steady state or remain quasi-periodic (tertiary waves). (13) When Rayleigh number increases there is onset of tertiary cells formation depending on Pr. (14) Experimental observations show cell merging and moving. (15) There exists a particular set of aspect ratios and Rayleigh numbers in laminar regime in which multiple cells are formed called the multicellular regime. (16) Use of sophisticated instruments (PIV) for carrying out experiments serve as a tool for validating the flow patterns obtained by the numerical results and provides a better insight into the physics of the flow. (17) Pressure work is the main factor for in formation and merging of cells. **Limitations**: (1) Research on high AR cavities ($AR > 40$) has not been addressed. (2) Paper is confined to a particular range of Rayleigh number. (3) Stream-vorticity equations were used to eliminate pressure term which plays a vital role in the instability analysis. (4) Reason for multicellular flow disappearing only for flow between 12.5 and 15 and then flow becoming turbulent. (5) Approximations were made by considering analogy with natural convection or forced convection on an isolated flat plate. (6) It was assumed that the local heat transfer conditions in the corners are independent of the height H of the plates. (7) Cell formation due to instability was not studied. (8) Variation of viscosity was not considered for boundary layer regime where temperature differences are high. (9) The physical reasons why there are upper and lower limits of Ra where multicellular flows can exist still remains undetermined. (10) Based on updated laminar-turbulent limit more aspect ratios need to be simulated at different Ra to extend Ra_{cl} (critical Rayleigh number above which instability sets in) and Ra_{cu} (critical Rayleigh number at which multiple cells disappear). (11) The aspect ratio considered was low due to which the difference in averaged Nusselt numbers did not depend on initial conditions (gradual and impulsive runs). (12) The aspect ratio considered is very small and most heat is carried by convection across the cavity in the top end region. Hence the averaged Nusselt number values for various Rayleigh number with unsteady flow differed very little to that without unsteadiness. In short the effect of flow instability on heat transfer was not observed. (13) The reason for increase in Nusselt number after a particular Rayleigh number where hydrodynamic instability occurs is not known especially for high ARs. The possible reasons may be because, the flow becomes turbulent, flow enters the boundary layer regime or because of some other phenomenon which is not known. (14) Under prediction of heat transfer coefficient is attributed to a finer grid requirement due to which the dynamics of the boundary layer could not be captured. (15) Experimental cavity was made of highly conducting top and bottom due to which validation of data with adiabatic boundary conditions may be over or underpredicted. (16) The reason for temperature fluctuations for high aspect ratio cavities ($H/L > 40$) were assumed due to unsteady flow or turbulence. A proper reasoning was not reported. This suggests that analysis of flow patterns for the particular range of AR considered, is needed which would give a clear picture about the physics of flow. (17) Equations were solved analytically.

[a] Assumptions, conclusions and limitations with numbers specified on next page.

Table 2A – Temperature differences considered for various width and Rayleigh number.

W	Ra				
	1.00E + 03	1.00E + 04	1.00E + 05	1.00E + 06	1.00E + 07
5.8	21.67				
15.9	1	10.53	105.3		
31.8		1.316	13.16		
63.5			1.65	16.5	
84.7			0.7	7	70

the literature. A good agreement with the literature data was found.

1.4. Motivation

The objective to minimize heat loss in double pane windows is trivial since diurnal variation in temperatures take place due to which the temperature differences increase and decrease throughout the day causing a change in Ra number. Literature review suggests that in recent years, considerable amount of research has been carried out to understand the flow patterns generated in these gaps, over wide range of Rayleigh number (Ra) ($g\beta\,\Delta T\,L^3/\nu\alpha$) which subsequently affects the heat transfer coefficient (h). Also some of the major issues which were noticed during the literature review were that only a few researchers (Elsherbiny et al., 1982; Yin et al., 1978; Wakitani, 1996) have carried out experimental investigation in high AR cavities ($AR \geq 40$) and for the Ra number range ($1000 \leq Ra \leq 10^7$). However, Tables 2A and 2B, however, show that Elsherbiny et al. (1982) considered specific gap widths and height. Similarly Yin et al. (1978) considered heights (497.5 mm $\leq H \leq$ 1000 mm) for gap widths (12.7 mm $\leq L \leq$ 101.6 mm). Elsherbiny et al. (1982) found that some of the correlations were weakly dependent on AR and strongly dependent on temperature difference while some were dependent on both AR and temperature gradient. Some issues which were not considered by the previous authors have been discussed in detail in Section 3. The objective of the present work is (a) to carry out CFD simulations for specific cases of experimental (Yin et al., 1978; Elsherbiny et al., 1982) and numerical investigations (Le Quéré, 1990; Wakitani, 1994; Lartigue et al., 2000) available in literature and validate the present code by finding the deviations between the code and the earlier experimental data, (b) develop an understanding of the progress in the CFD based heat transfer prediction methodology over the years, (c) carry out CFD simulations (after initial validation using earlier experimental data) for numerical investigation in a narrow range of gap of 5 mm $\leq L \leq$ 25 mm, and height of 100 mm $\leq H \leq$ 1000 mm, 20 K $\leq \Delta T \leq$ 100 K and validate the new CFD results with the existing correlations, (d) propose two correlations (a generalized correlation encompassing all the earlier data and a correlation for data used in present CFD simulations (5 mm $\leq L \leq$ 25 mm, and 10 mm $\leq H \leq$ 100 mm, 20 K $\leq \Delta T \leq$ 100 K) and (e) check the accuracy of both these correlations for the predictions in the given ranges of parameters. The objective of proposing a correlation is to incorporate the sensitivity of the height (H) for varying gap widths and temperature differences as considered in (a) and (b).

Table 2B – Temperature differences for various heights and widths.

H (mm)	L (mm)
640	5.8–84.7
673.1	63.5
762	63.5
763.2	31.8
806.13	15.9

2. Mathematical formulation

In the present work, the left wall of the vertical enclosure is maintained at a constant temperature (T_H) while the right wall is maintained at a constant temperature T_C, and ($T_H > T_C$). Following are the assumptions made in the present work:

1. Fluid is assumed to be incompressible and Newtonian. Due to the small magnitude of variation in pressure the density variation is very small and hence even air can be approximated as incompressible. Hence, the flows can be accounted for by buoyancy variation (Ganguli et al., 2007).
2. The flow is assumed to be two-dimensional.
3. All the working fluids are operated at temperature differences within Boussinesq approximation. The well-known Boussinesq equation has been employed and the density in the buoyancy term, is assumed to vary with the temperature according to the following relation:

$$\rho = \rho_0(1 - \beta(T - T_0)) \tag{1}$$

$$\beta = \left[\frac{1}{\rho}\left(\frac{\partial \rho}{\partial T}\right)\right] \tag{2}$$

4. Heat transfer by radiation has been neglected, as relatively low temperatures and the differences have been considered.
5. Length of the enclosure is sufficiently large so that a two-dimensional motion can be assumed.
6. Variation in properties of air as a function of temperature are assumed to follow the following relations: $\mu = A_i T + B_i$ (Incropera and Dewitt, 2002):

$$\text{For air}: \quad \mu = 5\,\text{E} - 08T + 2\,\text{E} - 06 \qquad (\text{kg m}^{-1}\,\text{s}^{-1}) \tag{3}$$

$$k = 8\,\text{E} - 05T + 0.0016 \qquad (\text{W m}^{-1}\,\text{K}^{-1}) \tag{4}$$

$$C_p = 0.07T + 985.5 \qquad (\text{J kg}^{-1}\,\text{K}^{-1}) \tag{5}$$

where A_i and B_i are constants and T is the absolute temperature. Values of properties of air have been summarized in Table 3.

2.1. Non-dimensional governing equations

The dimensionless length, aspect ratio, velocities, pressure, temperature and time are given by the expressions given

Table 3 – Properties of air.

Fluid	Air
Density ρ (kg m^{-3})	1.23E + 00
Specific heat C_p (J kg^{-1} K^{-1})	1.01E + 03
Dynamic viscosity μ (m^2 s^{-1})	1.79E − 05
Thermal conductivity k (W mK^{-1})	3.00E − 02
Thermal expansion coefficient β (K^{-1})	3.45E − 03

below.

$$X = \frac{x}{L}, \qquad Y = \frac{y}{L} \tag{6}$$

$$U = \frac{u}{V_0}, \qquad V = \frac{v}{V_0}, \qquad \text{where } V_0 = \sqrt{g\beta\,\Delta T\,L} \tag{7}$$

$$P = \frac{p}{\rho {V_0}^2}, \qquad \theta = \frac{T - T_m}{T_h - T_c}, \qquad t^* = \frac{t}{t_0}, \qquad \text{with} \quad t_0 = \frac{L}{V_0} \tag{8}$$

The transient governing equations (dimensional) are given comprehensively in Table 4. Table 4 also includes the initial and final temperature and velocity boundary conditions.

2.2. *Grid sensitivity*

The grid test has been performed for low value of AR (AR = 10) and highest and lowest values of Ra ($Ra = 10^7$, $L = 84.7$, $\Delta T = 70$ K, $Ra = 3.15E+05$, $L = 25$ mm, $\Delta T = 90$ K and $Ra = 2.52E+03$, $L = 5$ mm, $\Delta T = 90$ K). Three different grids namely (A) uniform grid 10×50, (B) Non-uniform grid 20×50 with 75% of the nodes near the walls with the first grid point at $x^+ = 0.1$ and (C) Non-uniform grid 20×50 with 50% of the nodes near the walls with the first grid point at $x^+ = 10$ is shown in Fig. 4 for $L = 5$ mm, AR = 10. The velocity profiles have been compared for a gap width of 5 and 15 mm for all the three cases as shown in Fig. 5A and B. A ±2% deviation has been observed in Case (C) as compared to Case (A) or Case (B). Further, Case (B) and (C) gave better results than the uniform grids (Case A) and for higher gap widths ($L = 12.5$, 15 and 20 mm) for $20 \le AR \le 100$ and higher ΔTs ($40\text{ K} \le \Delta Ts \le 70$ K). For multiple circulation cell formation the Case (C) gave the best results with reasonably accurate predictions (of heat transfer coefficients as reported in the present manuscript ±10%). Hence the grid defined in Case (C) was selected for further analysis.

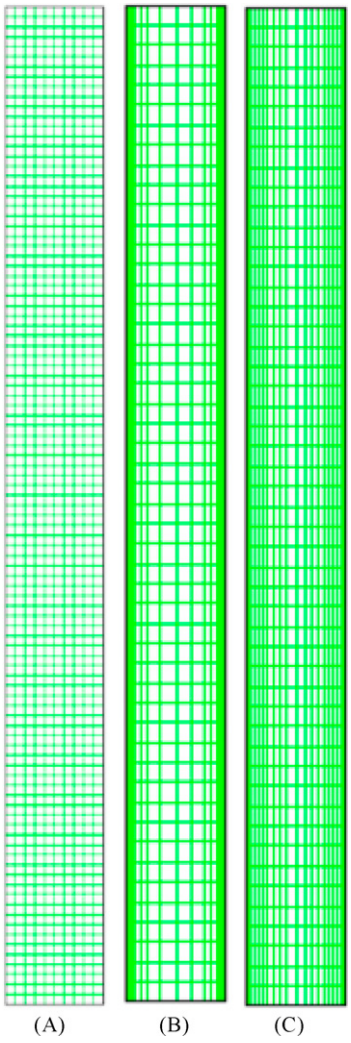

Fig. 4 – Schematic of the different grids considered for grid sensitivity: (A) uniform grid 10 × 50; (B) non-uniform grid 20 × 50 (75% of the nodes near the walls with the first grid point at $x^+ = 0.1$); (C) non-uniform grid (40% of the nodes near the walls with the first grid point at $x^+ = 10$).

2.3. *Method of solution*

The laminar model equations described above have been solved using commercial flow simulation software FLUENT

Table 4 – Boundary conditions and the model equations used for 2D model.

2D	Equations	Boundary conditions
Mass balance	$\rho\left(\frac{\partial u}{\partial x} + \frac{\partial v}{\partial y}\right) = 0$	Initial velocity condition: $u(x, y, 0) = v(x, y, 0) = 0$ for $0 \le x \le L$ $0 \le y \le H$ Initial temperature condition: $T(x,y,0) = 0$ for $0 \le x \le L$ $0 \le y \le H$
Momentum balance	In x-direction $\rho\left(\frac{\partial u}{\partial t} + u\frac{\partial u}{\partial x} + v\frac{\partial u}{\partial y}\right) = -\frac{\partial p}{\partial x} + \left\{\frac{\partial}{\partial x}\left[\mu\frac{\partial u}{\partial x}\right] + \frac{\partial}{\partial y}\left[\mu\frac{\partial u}{\partial y}\right]\right\}$	Initial x-direction boundary conditions: $u(x, 0, t) = v(x, 0, t) = 0$ for $0 \le x \le L$ and $t \ge 0$ Final x-direction boundary conditions: $u(x, 0.4, t) = v(x, 0.4, t) = 0$ for $0 \le x \le L$ and $t \ge 0$ Final y-direction boundary conditions: $u(0, y, t) = v(0, y, t) = 0$ for $0 \le y \le H$ and $t \ge 0$ Final y-direction boundary conditions: $u(L, y, t) = v(L, y, t) = 0$ for $0 \le y \le H$ and $t \ge 0$
	In y-direction $\rho\left(\frac{\partial v}{\partial t} + u\frac{\partial v}{\partial x} + v\frac{\partial v}{\partial y}\right) = -\frac{\partial p}{\partial y} + \left\{\frac{\partial}{\partial x}\left[\mu\frac{\partial v}{\partial x}\right] + \frac{\partial}{\partial y}\left[\mu\frac{\partial v}{\partial y}\right]\right\} + g\beta\,\Delta T$	$T_c = 300$ $320 < T_H < 410$ for $0 \le y \le H$ and $t = 0$ $T_c \le T(L, y, t) < T_H$ for $0 \le y \le H$ and $t \ge 0$
Energy balance	$\frac{\partial T}{\partial t} + u\frac{\partial T}{\partial x} + v\frac{\partial T}{\partial y} = \alpha\left(\frac{\partial^2 T}{\partial x^2} + \frac{\partial^2 T}{\partial y^2}\right)$	$\frac{\partial T(x,0,t)}{\partial y} = \frac{\partial T(x,H,t)}{\partial y} = 0$ for $0 \le x \le L$ and $t \ge 0$

Table 5 – Table showing discretization scheme independency.

H	AR	Ra	Heat Transfer Coefficient (W/m^{2}K)		
			Third-order MUSCL scheme	Second-order upwind scheme	QUICK scheme
100	20	559.278	2.5	2.48	2.5
100	10	4474.23	2.38	2.38	2.38
100	8	8738.72	2.26	2.25	2.25
100	6.66667	15100.5	2.23	2.24	2.23
100	5	35793.8	2.21	2.2	2.22
100	4	69909.8	2.202	2.2	2.22
500	100	1677.83	3.02	2.99	3
500	50	13422.7	2.37	2.32	2.35
500	40	26216.2	2.315	2.3	2.32
500	33.3333	45301.5	2.281	2.28	2.28
500	25	107381	2.32	2.29	2.3
1000	200	1677.83	2.69	2.65	2.68
1000	100	13422.7	2.193	2.19	2.19
1000	80	26216.2	2.098	2.1	2.09
1000	66.6667	45301.5	2.025	2.021	2.025
1000	50	107381	2.01	2	2.013

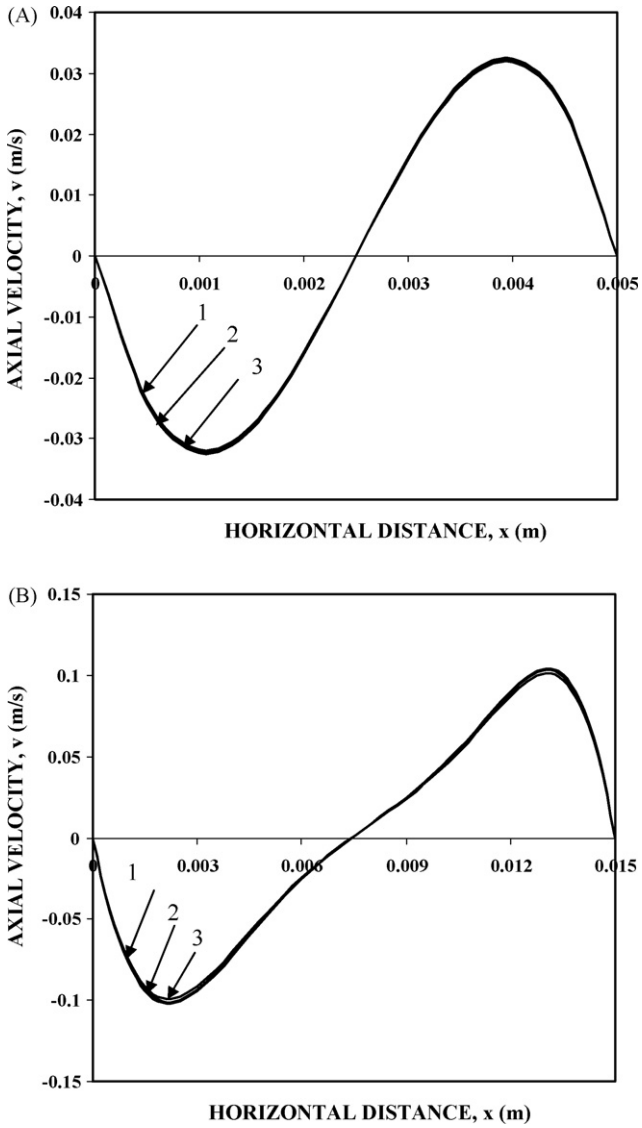

Fig. 5 – Variation of axial velocity across horizontal distance. (A) L = 5 mm, AR = 10. Ra = 2.52E + 03. L = 15 mm, AR = 10: (1) uniform grid 10 × 50; (2) non-uniform grid 20 × 50 (75% of the nodes near the walls with the first grid point at $x^+ = 0.1$); (3) non-uniform grid (40% of the nodes near the walls with the first grid point at $x^+ = 10$).

(version 6.2.16) (FLUENT, 2005). Transient simulations have been carried out with a time step of 0.0001 s. For each time step, convergence criteria for sum of normalized residues have been set to 1×10^{-4} for continuity equations, 1×10^{-4} for momentum and 1×10^{-7} for energy equations. Convergence has been ensured at every time step. The continuity equation has been converged for each timestep so that the mass balance is satisfied while the heat flux at the cold and hot wall was found to be equal in magnitude and opposite in direction (Heat in = Heat out) to satisfy energy balance. Thus a steady state situation has been ensured. For a quasiperiodic situation, simulations have been carried out for long time duration to ensure proper energy balance to be satisfied (Ganguli et al., 2007). The under-relaxation parameters were set to 0.3 for pressure, 1 for density, energy and body forces and 0.7 for momentum equations. In this study, a segregated solver with implicit time discretization has been employed for obtaining the solution of momentum equations. The discretization scheme independency was checked for different gap widths (5 mm ≤ L ≤ 25 mm), (100 mm ≤ H ≤ 1000 mm), (20 K ≤ ΔT ≤ 60 K) as shown in Table 5. Three discretization schemes were used namely second-order upwind scheme, QUICK scheme and the third-order MUSCL scheme. The deviation in averaged heat transfer coefficient has been found to be less than 1%. Although, the momentum equations in the present work were discretized using the third-order monotone upstream centered schemes for conservation laws (MUSCL) scheme, the other two schemes of commercial software FLUENT 6.2.16, can also be used for discretization.

3. Results and discussion

3.1. *Comparison of results of CFD simulations of the present work with literature data*

CFD simulations were carried out for 16 ≤ AR ≤ 40, 3.55E + 03 ≤ Ra ≤ 2E + 04 as used in the earlier literature (Le Quéré, 1990; Zhao et al., 1997; Lartigue et al., 2000). The number of cells obtained by the present code, shows an excellent match with the ones obtained from the literature as can be seen from Fig. 6.

The comparison of the predictions from CFD simulations for geometries of Batchelor (1954), Newell and Schmidt (1970), Yin et al. (1978), Elsherbiny et al. (1982), Lee and Korpela (1983)

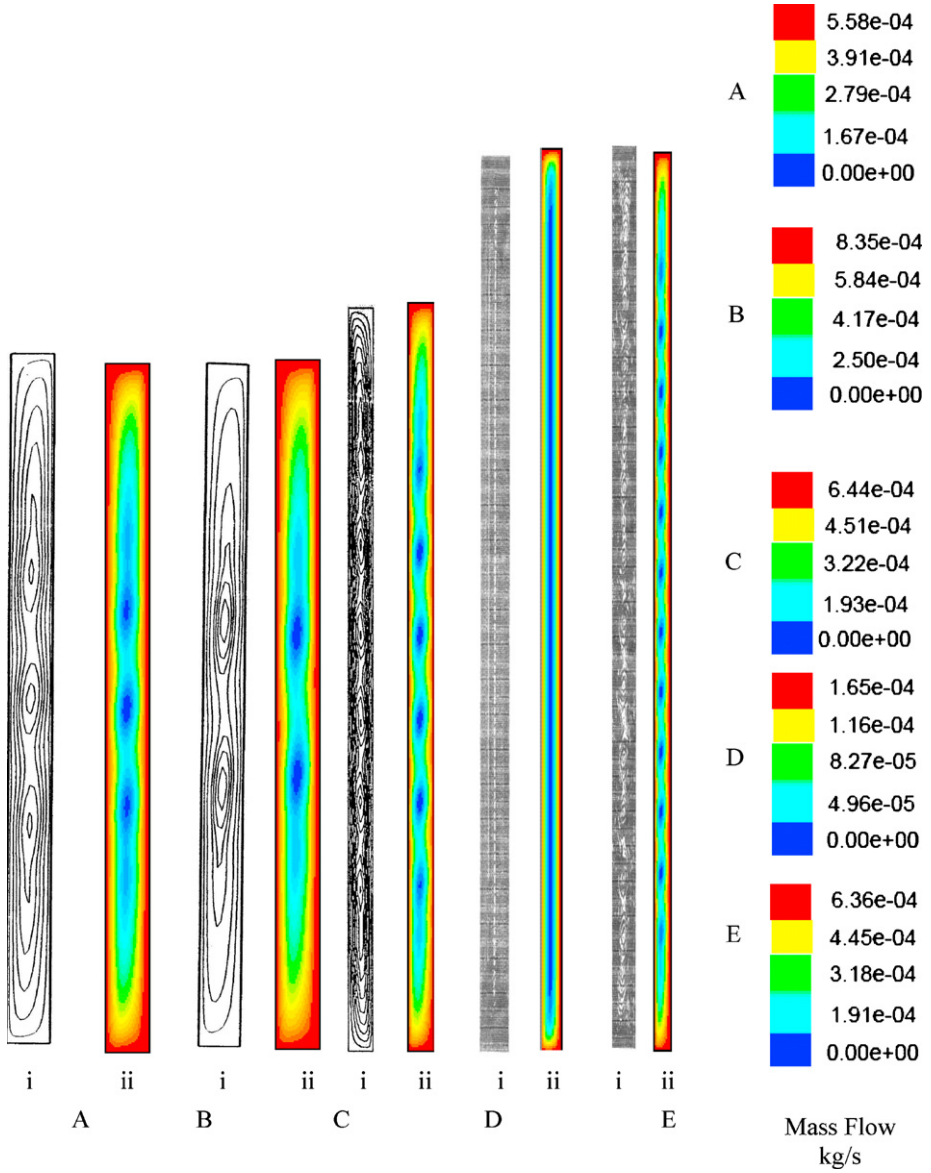

Fig. 6 – Flow patterns found by different authors. (A) AR = 16, *Ra* = 12,000: (i) Le Quéré (1990) and (ii) present work. (B) AR = 16, *Ra* = 20,000: (i)Le Quéré (1990) and (ii) present work. (C) AR = 25, *Ra* = 10,100: (i) Zhao et al. (1997) and (ii) present work. (D) AR = 40, *Ra* = 3550: (i) Lartigue et al. (2000) and (ii) present work. (E) AR = 40, *Ra* = 14,200: (i) Lartigue et al. (2000) and (ii) present work.

with their own data is presented in Fig. 7A–E for all *Ra* numbers used in their work. The variation of *Nu* number with *Ra* number in an ascending order of AR is as follows.

Fig. 7A shows the variation of *Nu* number with *Ra* number for AR = 5. The present numerical simulations show very good agreement with the experimental results of Elsherbiny et al. (1982) and numerical predictions of Lee and Korpela (1983) with a deviation of only ±1%. The predictions of the present simulations are slightly higher (by 10%) as compared to the numerical predictions of Newell and Schmidt (1970). Further, the present numerical predictions overestimate *Nu* number (by 10%) as compared to the experimental results of Yin et al. (1978).

Fig. 7B shows the variation of *Nu* number with *Ra* number for AR = 10. The present numerical simulations overestimate the Nusselt number values, as compared to the predictions of Batchelor (1954) (by 10%) while it shows a good agreement with the experimental results of Elsherbiny et al. (1982). For the same AR, the present simulations show an excellent agreement with the numerical simulations of Lee and Korpela (1983). An overestimation (by 7%) was observed when the present numerical results are compared with the numerical predictions of Newell and Schmidt (1970).

Fig. 7C shows the variation of *Nu* number with *Ra* number for AR = 20. The differences observed between the present results and analytical predictions of Batchelor (1954) are as follows: for low Rayleigh numbers ($Ra \leq 6 \times 10^4$) the *Nu* numbers predicted in the present work are higher (by 10%) as compared to Batchelor (1954) while for higher Rayleigh numbers ($Ra \geq 6 \times 10^4$) current predictions are lower as compared to Batchelor (1954) (by 10%). Further, for the case of AR = 20, the present predictions show an excellent match with the experimental results of Elsherbiny et al. (1982); and with the numerical simulations of Lee and Korpela (1983) at lower *Ra* numbers ($Ra \leq 1 \times 10^4$) while 5% overestimate as compared to the *Nu* number predictions of Lee and Korpela (1983) at higher *Ra* numbers have been observed. Further, the present simulations overestimate (by 5%) when compared to the numerical predictions of Newell and Schmidt (1970).

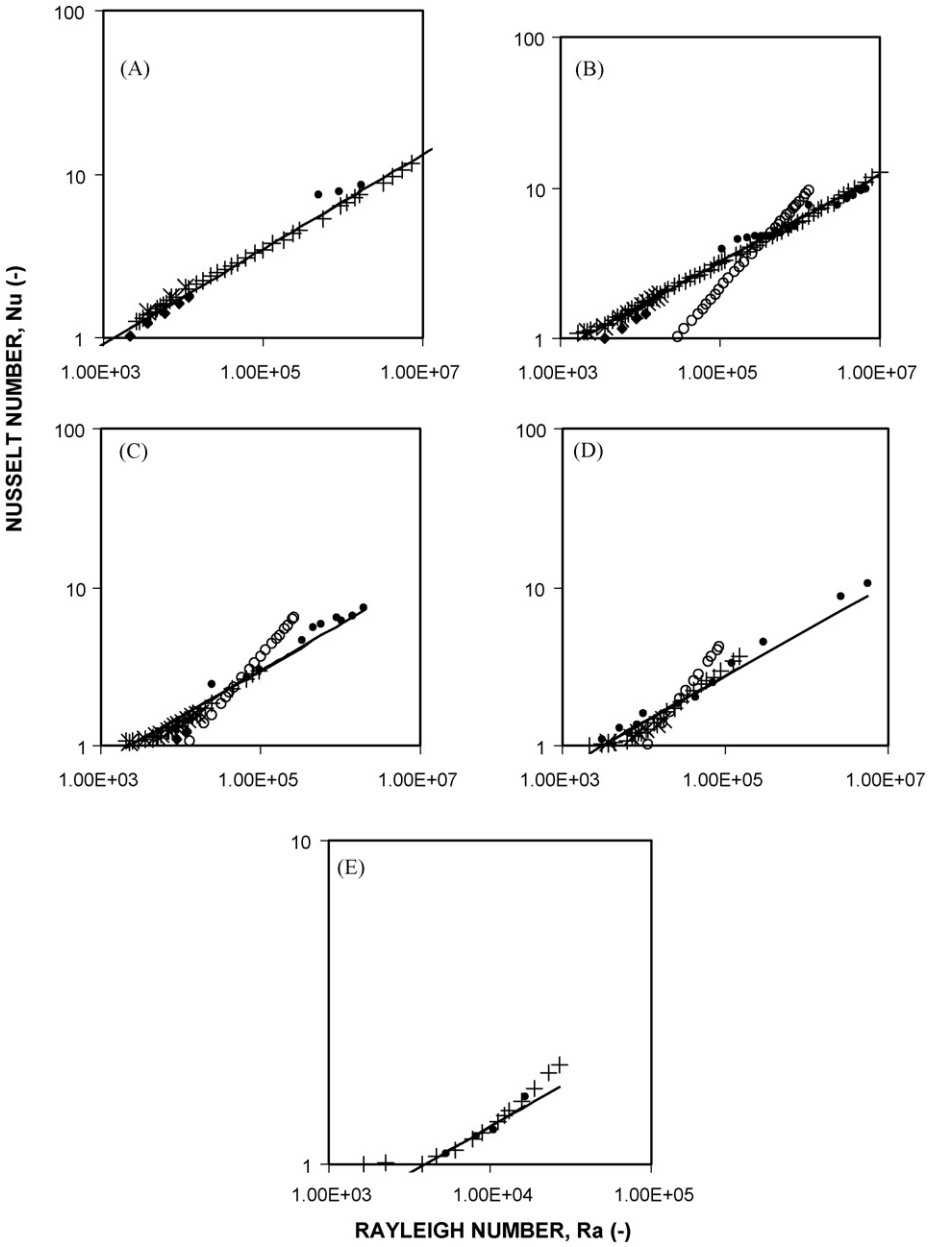

Fig. 7 – Variation of Nusselt number with Rayleigh number for various aspect ratio for various authors: (○) Batchelor, Theoretical (1954); (♦) Newell and Schmidt, Theoretical (1970); (●) Yin et al. Experimental (1978); (+) Elsherbiny et al., Experimental (1982); (*) Lee and Korpela, Theoretical (1983). (A) AR = 5, (B) AR = 10, (C) AR = 20, (D) AR = 40 and (E) AR = 80.

Fig. 7D shows the variation in *Nu* number with *Ra* number for AR = 40. The present work underestimates *Nu* when compared with the results of Batchelor (1954), while they show a good agreement with the experimental results of Elsherbiny et al. (1982). Further, the present predictions overestimate *Nu* number (by 2%) as compared with the numerical predictions of Lee and Korpela (1983) for ($Ra \geq 2.5 \times 10^4$). The present simulations underestimate *Nu* by 10% when compared with of the experimental results of Yin et al. (1978).

For a very high AR = 80 the data matches well with Elsherbiny et al. (1982) with a slight underestimation (by 5%) while the present simulations again underestimate (by 3%) when compared with the results of Yin et al. (1978) (Fig. 7E).

The main reasons for the overestimations or underestimations (±15%) of the present simulations as compared to the literature are as follows: Batchelor (1954) used stream vorticity equations to eliminate the pressure term. The importance of pressure, responsible for the onset of flow instability (boundary layer breaking up and formation of flow cells) at high *Ra* numbers ($Ra \geq 5 \times 10^4$) has been extensively investigated (Chan et al., 2004; Ganguli et al., 2007). Pressure differences, although low in magnitude play a significant role in the evolution of the flow patterns which in turn affect the heat transfer (Chan et al., 2004; Ganguli et al., 2007). Batchelor (1954) neglected the pressure difference produced by gravity, since they are small as compared to the absolute pressure. Further, he analyzed the flow over a single vertical plate and the presence of the second vertical plate (which forms rectangular cavity) was neglected. AR plays a significant role in the prediction of heat transfer coefficient. Newell and Schmidt (1970) considered a low range of AR ($5 \leq AR \leq 20$). A better grid sensitivity analysis in the present work is the reason for the deviations obtained for the range covered by Newell and Schmidt (1970). Fig. 8 shows, that the finer nonuniform grid (Case C, Section 2.3) gives better estimates of the velocity distribution which is likely to enhance the accurate prediction of

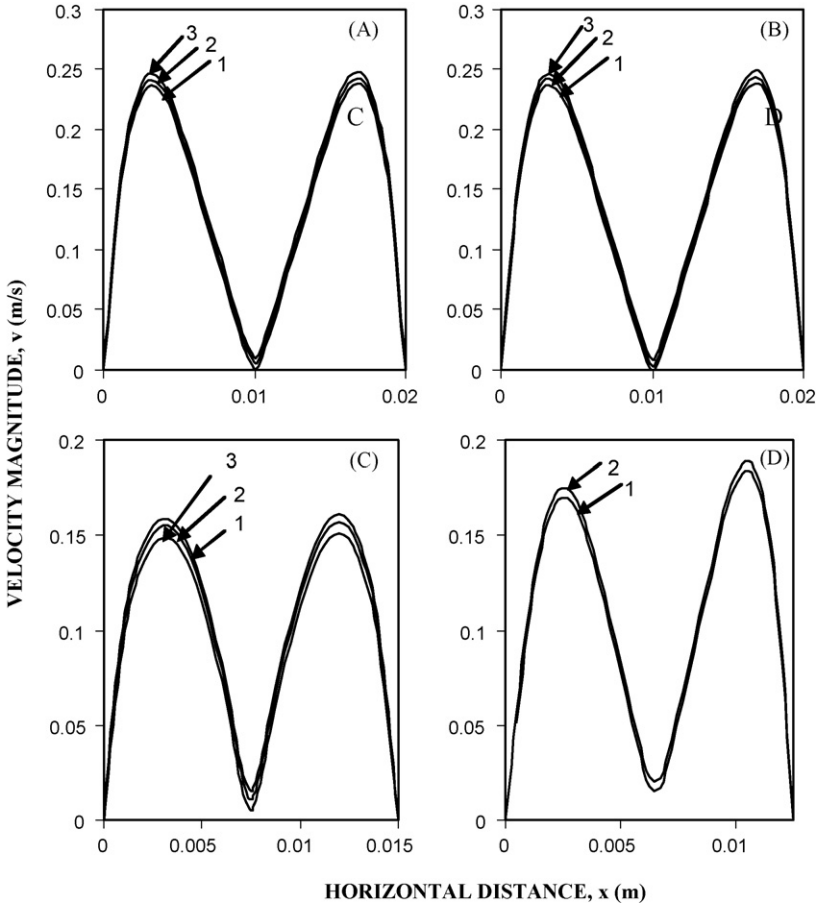

Fig. 8 – Effect of grid size on velocity distribution at $x/H = 0.5$: (1) Newell and Schmidt (1970); (2) Lee and Korpela (1983); (3) present study. (A) AR = 10, (B) AR = 12, (C) AR = 20 and (D) AR = 24.

the heat transfer coefficient (HTC). As per the grid sensitivity analysis in Section 2.3 the grid of Case C has been compared with the grid specifications of Newell and Schmidt (1970) and the deviations are found to be less than 4%. The conditions and the values of Yin et al. (1978) are over-estimated by the present numerical scheme due to the following reasons: (a) Yin et al. (1978) assumed that the magnitude of radiative heat transfer ranged from 7 to 17% of the power input and (b) heat loss due to conduction through spacers was found to be 5% of total power input thus accounting for the observed deviations observed in this work. Deviation from results of Lee and Korpela (1983) is attributed to a still finer grid requirement near the walls due to which the dynamics of the boundary layer could not be captured by Lee and Korpela (1983).

3.2. *Effect of flow patterns on heat transfer for varying height and gap width*

In the previous subsection we have discussed the shortcomings of the previous investigators and validation of the CFD code developed in this work. In this subsection we try to understand the effect of fluid flow and patterns on heat transfer. Fig. 9A and B illustrates the variation in HTC at the hot wall for different gap widths ($W = 5$, 10, 20; $H = 100$ mm; $\Delta T = 60$ K) and heights ($H = 300$, 500, 1000; $L = 15$ mm; $\Delta T = 60$ K). The discussion of Fig. 9A and B is given in the later part of the text of this subsection. Consider the first case of height 100 mm and gap widths ($W = 5$ mm, 10 mm, 12.5, 15, 20 mm). The flow patterns from Fig. 10 A–E show that there is a unicellular flow pattern for all the gap widths. The HTC's at the top and bottom portion of the enclosures are, however, four times higher than in the rest of the enclosure as can be observed in Fig. 9A. With an increase in gap width ($W = 10$ mm) though mixing at the top and bottom portion increases with a corresponding increase in local HTC, the HTC in the rest of the enclosure remains low. Thus the average HTC is low and overall heat loss decreases. But with a further increase in gap width ($W = 15$ or 20 mm) the pattern of decrease in HTC remains the same and the overall HTC remains more or less the same (Fig. 9A). Hence with further increase in gap width there is no effective reduction in heat loss. We now try to understand what happens when we increase the height from $H = 100$ mm to $H = 300$ mm. Fig. 10F–I shows that as we increase the height ($H = 300$ mm) for lower gap widths ($L = 5$ mm) unicellular pattern occurs while for higher gap widths ($L = 10$ mm) instability takes place and steady multiple cell formation occurs. With an increase in the height the effective area for heat transfer increases and temperature gets distributed over a larger area due to which the average HTC is lower than that for an enclosure having lower height. However, when transition from unicellular to multicellular pattern takes place, the local HTC's are enhanced due to fluctuations (as seen in Fig. 9B) resulting in an effective increase in average HTC. If we move our focus on higher heights (like $H = 500$ and 1000 mm; $L \geq 12.5$ mm (refer Fig. 9B)) the enhancement in heat transfer for such cases is mainly due to the multiple cell formation in the central part of the enclosure. This is due to the moving and merging of the cells. A good discussion on this unsteady phenomenon can be found in the literature (Lee and Korpela, 1983; Ganguli et al., 2007). Fig. 9B shows the variation in local HTC with height ($H = 500$

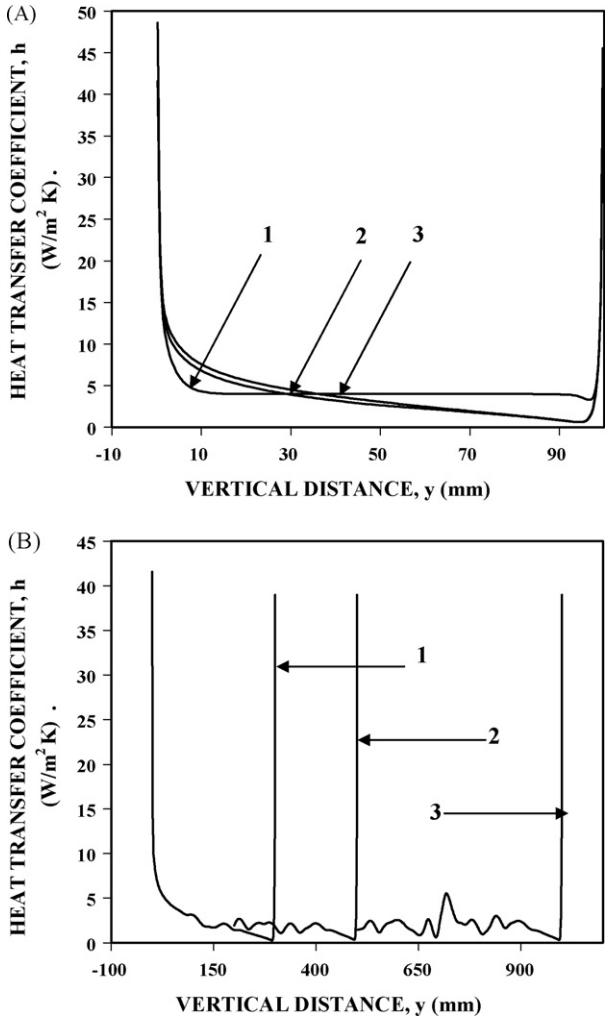

Fig. 9 – Variation of heat transfer coefficient with vertical distance. (A) H = 100 mm: (1) L = 5 mm; (2) L = 10 mm; (3) 20 mm. (B) L = 15 mm: (1) H = 300 mm; (2) H = 500 mm; (3) H = 1000 mm.

and 1000 mm; L = 15 mm (peaks numbered as 2 and 3 in Fig. 9B)) while Fig. 10J and K shows multicellular patterns for the same cases. From Fig. 9B it can be observed that the local HTC's at the top (y = 496–500 mm) for H = 500 mm ($h \leq 35\,W\,m^{-2}\,K^{-1}$) and at the bottom ($y$ = 0–18 mm) is $h \leq 50\,W\,m^{-2}\,K^{-1}$, respectively, while in the central part it is in the range of $h \leq 5\,W\,m^{-2}\,K^{-1}$. Similarly for H = 1000 mm the local HTC's at the top (y = 996–1000 mm) is $h \leq 25\,W\,m^{-2}\,K^{-1}$ and at the bottom (y = 0–18 mm) is $h \leq 50\,W\,m^{-2}\,K^{-1}$, respectively, while in the central part it is in the range of $h \leq 5\,W\,m^{-2}\,K$. Thus, we can conclude that considerable mixing takes place in the central part and bottom of the enclosure. Further, the mixing at the top part of the enclosure is much less in enclosures having higher heights (500 mm $\leq H \leq$ 1000 mm) as compared to that for lower heights (100 mm $\leq H \leq$ 300 mm). One can also draw the conclusion that with low mixing rates and lower htc's (50% as compared to H = 100 mm) at the top for higher heights (500 mm $\leq H \leq$ 1000 mm) had there been no steady multicellular pattern or merging and moving multicellular pattern as observed, the average HTC would have been lower by at least approximately 5%. Even a 5% decrease is a significant decrease in HTC due to a large contribution from heat transfer area. The above calculations also go for L = 15 mm. For higher gap widths the HTC would go on decreasing. Thus with increase in gap width the HTC would decrease. However, due to multicellular cell formation a continuous decreasing trend in HTC is not observed but a constant value is observed. Thus it has been validated that multicellular cell formation causes enhancement in HTC which in turn causes no decrease in heat loss after a certain gap width.

Now we consider different temperature differences (ΔT = 20, 40, 60, and 90 K) and see the effect of variation of height and gap width on the HTC. Fig. 11 shows the variation in HTC for 5 mm $\leq L \leq$ 25 mm and 100 mm $\leq H \leq$ 1000 mm. It is a well-known fact that HTC decreases with height for a constant gap width but the trends of change in HTC with gap width varies for different temperature gradients. Fig. 11A shows that for ΔT = 20 K the optimum gap width for any height will be between 10 and 15 mm and the HTC remains constant after 20 mm. Due to a comparatively low temperature gradient the formation of multiple cells starts at a higher gap width and hence maximum insulation can be achieved at a gap width up to 15 mm. For ΔT = 40 K as shown in Fig. 11B at lower heights (H = 100 and 300 mm) the lowest HTC is at L = 12.5 mm after which the HTC remains constant. For higher heights (H = 500, 800, and 1000 mm) the lowest HTC is in the range 12.5 mm $\leq L \leq$ 13.5 mm again. The flow patterns, however, show the formation of multiple cells after L = 12 mm. This means that the enhancement in the heat transfer coefficient also depends upon the circulation strength of the circulation cells that are formed. In the range 11 mm $\leq L \leq$ 13.5 mm the steady multiple circulation cells are formed. For $L \geq$ 13.5 mm the moving and merging of cells starts, appearing due to which the mixing rates enhances reducing temperature gradients and hence the reduction in heat loss does not occur as the overall temperature gradient reduces. An important aspect to be noted here is that there is unsteady flow behavior due to moving and reforming of cells. The boundary layer thickness at both the walls tend to reduce due to this cell merging and moving phenomena. Due to the reduction in thickness of the thermal boundary layer the resistance to the transfer is lowered and the averaged HTC at the hot wall increases over a short time duration. Thus, due to cell merging and moving the time-averaged HTC is enhanced. Fig. 12 clearly depicts this increase when moving and merging of cells occur for AR = 40 and $Ra = 1 \times 10^5$. Hence to understand the values of Ra number and AR at which the flow transition regime starts, the velocity at a point near the hotwall of the enclosure has been considered. The results were interesting, confirming the observations reported in the literature (Zhao et al., 1997) which show that the HTC increases due to the formation of cellular flow patterns. Similarly, for higher temperature differences (ΔT = 60 and 90 K) the optimum gap width of H = 100 mm is L = 10 mm while for 300 mm $\leq H \leq$ 1000 mm the gap width is L = 12.5 mm. For a height of H = 500 mm the HTC increases after L = 15 mm. This again explains that for a specific height the mixing rates in the central part may be different and hence the optimum gap width needs to be chosen with care. For higher temperature differences like (ΔT = 90 K) for all $H \geq$ 300 mm the HTC increases after L = 12.5 mm. Thus the selection of proper gap width corresponding to the height as well as the temperature gradient is very important.

3.3. *Temperature distribution*

Understanding the fluid dynamics in the entire enclosure is possible by estimating the temperature distribution in the enclosure. Fig. 13A, C, and E shows that there is a linear temperature distribution in the entire region of the enclosure

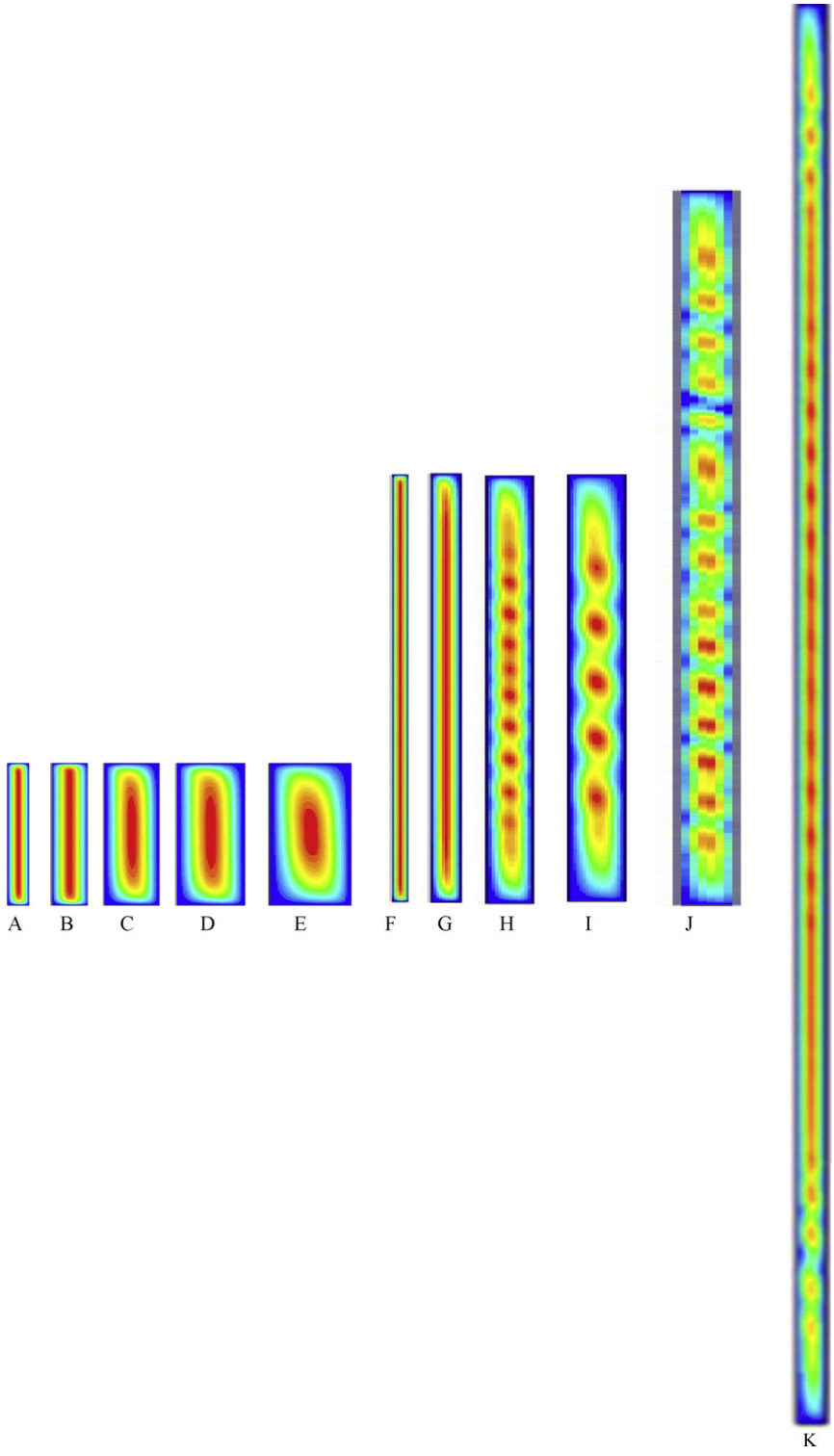

Fig. 10 – Flow patterns for various widths. (A) $H = 100$ mm and $L = 5$ mm; (B) $H = 100$ mm and $L = 8$ mm; (C) $H = 100$ mm and $L = 10$ mm; (D) $H = 100$ mm and $L = 15$ mm; (E) $H = 100$ mm and $L = 20$ mm; (F) $H = 300$ mm and $L = 5$ mm; (G) $H = 300$ mm and $L = 10$ mm; (H) $H = 300$ mm and $L = 12.5$ mm; (I) $H = 300$ mm and $L = 15$ mm; (J) $H = 500$ mm and $L = 15$ mm; (K) $H = 1000$ mm and $L = 12.5$ mm.

suggesting that heat from the hot wall to the cold wall is transferred by conduction. There is a significant drop in the heat transfer rate with an increase in the gap width since it follows Fourier's law of heat conduction. Fig. 13B shows the temperature profiles for AR = 20 and $Ra_L = 8.32 \times 10^3$. The temperature gradient in the core becomes slightly flatter and non-linear suggesting that the dominance of conduction is reduced due to a small amount of convection setting up in the core part. When only conduction is the mode of heat transfer, the rate of heat transfer per unit area decreases with an increase in the resistance (gap width of the enclosure), but when fluid is convected, it promotes heat transfer and after a certain critical resistance, the rate of heat transfer does not show a significant decrease and becomes constant. The temperature profile of Fig. 13B is representative of all the figures having flow patterns where convection promotes heat transfer. Fig. 13D shows a steep vertical temperature gradient near the wall. This confirms the existence of the cellular patterns formed

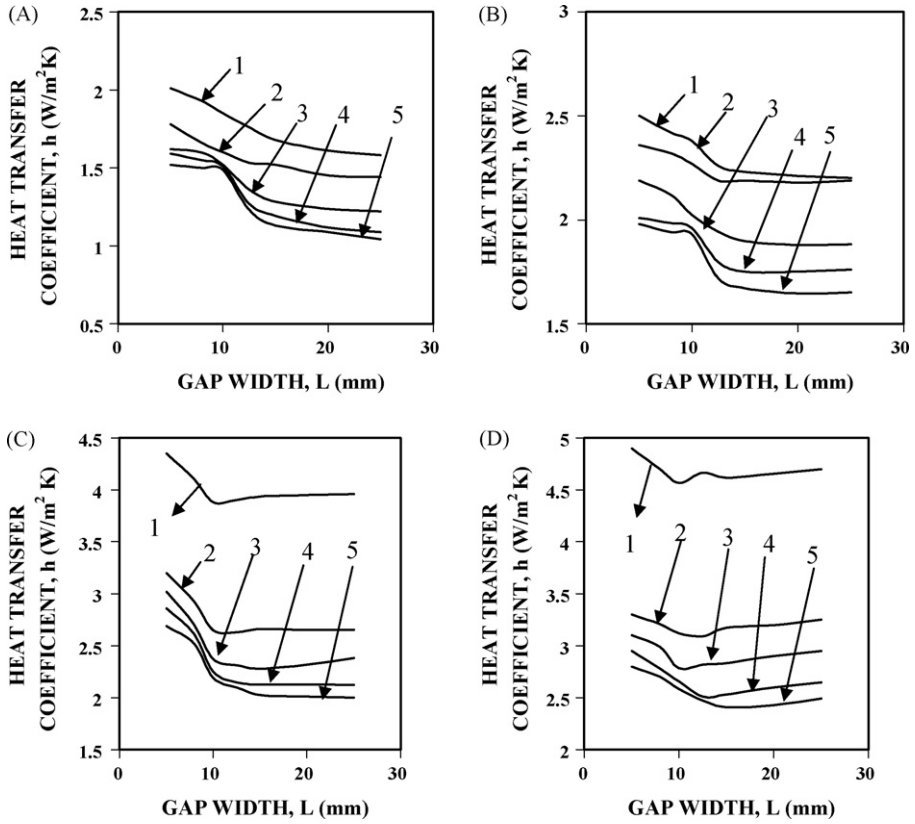

Fig. 11 – Variation of heat transfer coefficient with gap width: (A) Temperature difference $\Delta T = 20$ K; (B) $\Delta T = 40$ K; (C) $\Delta T = 60$ K; (D) $\Delta T = 90$ K. (1) $H = 100$ mm; (2) $H = 300$ mm; (3) $H = 500$ mm; (4) $H = 800$ mm; (5) $H = 1000$ mm.

inside the enclosure which increases the rate of heat transfer. This regime is the transition regime in which the boundary layer flows formed at the hot and cold plate reach the central part of enclosure core and meet each other. Hence, there is a rotary motion of the fluid, causing mixing and enhancement in heat transfer. Fig. 13 B, D, F and I all show similar temperature profiles showing varying degree of steepness in the vertical temperature gradient near the wall and interference with each other. This forms the basis for the fact that there is an enhancement in time averaged heat flux than the one obtained by pure conduction mode. Fig. 13 H, J and L show the core to be nearly isothermal (flat of no temperature gradient) with the temperature gradient nearly equal to zero. This suggests that the transfer of heat is controlled by the moving boundary layers near the walls and the flow is in the laminar boundary layer regime. The heat transferred through the core is negligible as the gap width is increased due to negligible temperature gradients.

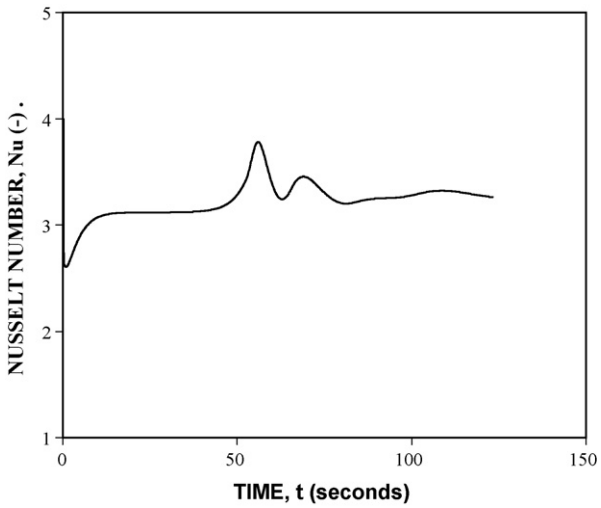

Fig. 12 – Variation of *Nu* number with time (AR = 40 and $Ra = 10^5$).

3.4. *Proposed correlation and its sensitivity analysis*

3.4.1. *Correlation development*

A generalized correlation has been proposed for range $5\text{ mm} \le L \le 84\text{ mm}$; $5\text{ K} \le \Delta T \le 105.3\text{ K}$; $100\text{ mm} \le H \le 1000\text{ mm}$ using regression analysis:

$$Nu = 0.171(Ra)^{0.265}(\text{AR})^{-0.205} \quad \text{(average deviation of } \pm 20\%) \tag{9}$$

Another correlation has been proposed for a lower range of $5\text{ mm} \le L \le 25\text{ mm}$; $20\text{ K} \le \Delta T \le 90\text{ K}$; $100\text{ mm} \le H \le 1000\text{ mm}$ as follows; with regression analysis giving better accuracy and prediction:

$$Nu = 0.151(Ra)^{0.3}(\text{AR})^{-0.164} \quad \text{(average deviation of } \pm 10\%) \tag{10}$$

The discussion on the variation in exponents and the reasons for it has been given the following subsection.

3.4.2. *Sensitivity analysis*

Fig. 14 shows a parity plot of the HTC derived from various correlations available in the literature as well as the experimental data with the generalized predicted correlation from the present work (Eq. (9)). The literature data shows a maximum deviation of ±20% from the present predictions.

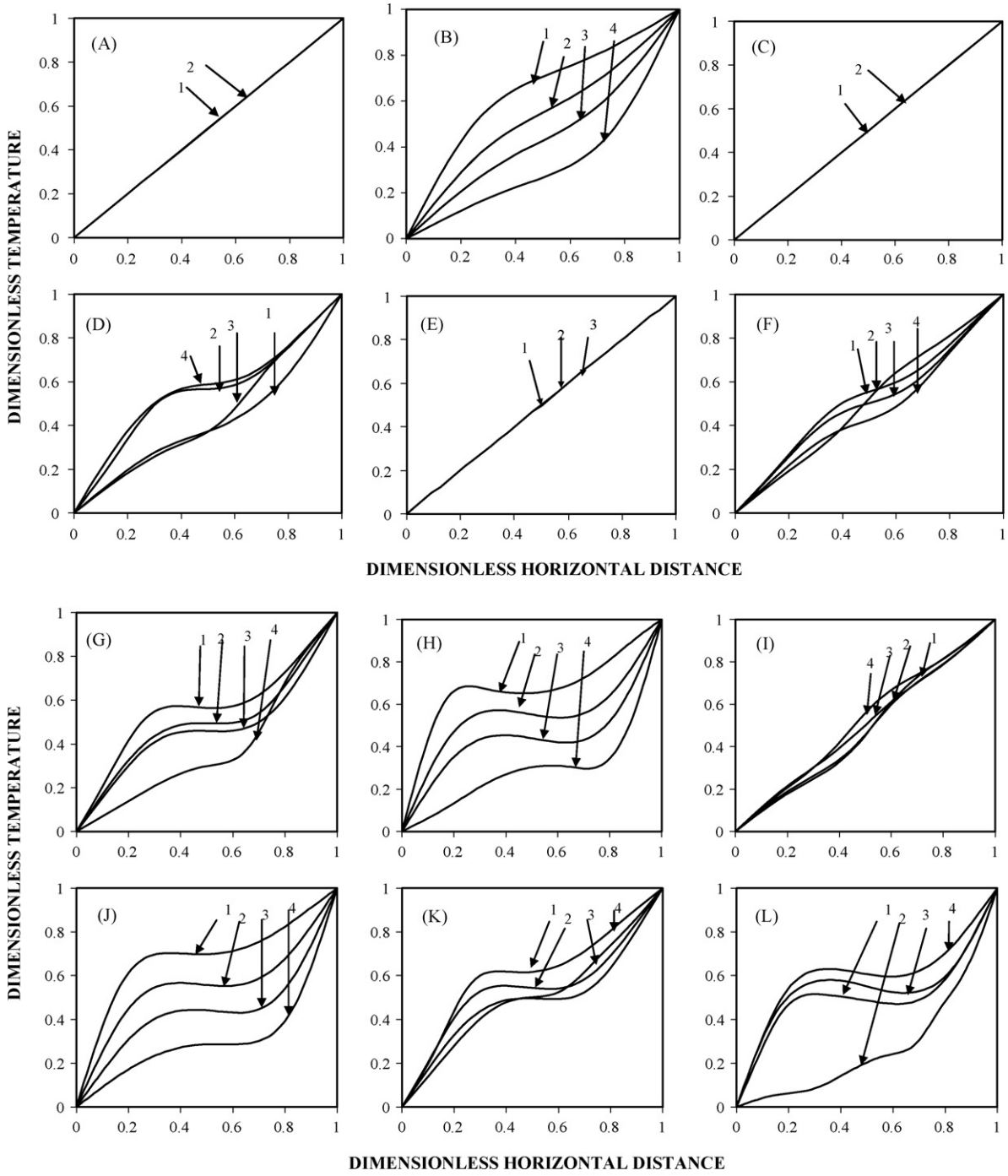

Fig. 13 – Temperature profiles varying with axial distance: (A) $H = 100$ mm, AR = 10, $L = 5$ mm and $Ra_L = 1.04 \times 10^3$; (B) $H = 100$ mm, AR = 20, $L = 10$ mm $Ra_L = 8.32 \times 10^3$; (C) $H = 300$ mm, AR = 60, $L = 5$ mm, $Ra = 1.04 \times 10^3$; (D) $H = 300$ mm, AR = 24, $L = 12.5$ mm; $Ra_L = 1.625 \times 10^4$; (E) $H = 500$ mm, AR = 62.5, $L = 8$ mm, $Ra = 1.04 \times 10^3$; (F) $H = 500$ mm, AR = 50, $L = 10$ mm, $Ra = 8.32 \times 10^3$; (G) $H = 500$ mm, AR = 33.33, $L = 15$ mm, $Ra = 2.808 \times 10^4$; (H) $H = 500$ mm, AR = 50, $L = 25$ mm, $Ra = 1.3 \times 10^5$; (I) $H = 800$ mm, AR = 64, $L = 12.5$ mm, $Ra = 1.625 \times 10^4$; (J) $H = 800$ mm, AR = 32, $L = 25$ mm, $Ra = 1.3 \times 10^5$; (K) $H = 1000$ mm; AR = 15.625, $L = 15$ mm, $Ra = 2.808 \times 10^4$; (L) $H = 1000$ mm, AR = 32, $L = 25$ mm, $Ra = 1.3 \times 10^5$. (1) $y/H = 0.2$; (2) $y/H = 0.4$; (3) $y/H = 0.6$; (4) $y/H = 0.8$.

Experimental data of Elsherbiny et al. shows a minimum deviation with an error of −5%. Correlation of Jakob (1949) also shows very good match with a deviation of 8%. The deviation with the experimental data of Yin et al. (1978) was high of about 20% while that of Eckert and Carlson (1961) was about 25%. The deviation of correlation of Newell and Schmidt (1970) was about 20%. Some of the reasons for the deviation have already been discussed before. Since the generalized correlation encompasses all the data for a large number of gap widths, heights and temperature differences (180 combinations for cases considered in this work and 295 cases from literature) the deviations are large. Some of the important aspects of the present correlation in this work have been the consideration of effect of height for each gap width considered. For example, if we consider a height of 100 mm and a gap width of 5 mm we also get AR = 20 while for $H = 500$ mm and $L = 25$ mm we get the same AR. However, these different combinations of AR give a different exponent over AR by regression and the exponent over AR makes a lot of difference while predicting the heat transfer coefficient. The exponent over Ra is

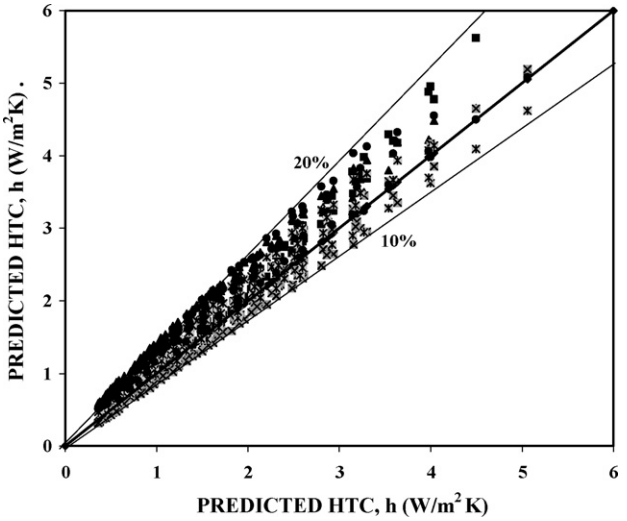

Fig. 14 – Parity plot of predicted heat transfer coefficient for correlation given by Eq. (9): (■) Newell and Schmidt (1970) (Numerical); (▲) Yin et al. (1978) (Experimental); (♦) Eckert and Carlson (1961) (Experimental); (✱) Jakob (1949) (Experimental); (✱) Elsherbiny et al. (1982).

seen to vary between 0.25 and 0.31 in the literature while that of AR varies from −0.11 to −0.27. This suggests that an independent consideration of various combinations of heights and gap widths (for same AR) will give us better understanding of variation in heat transfer coefficient. With an increase in the field of CFD the effect of flow on heat transfer can also be understood making such comprehensive number of runs numerically. The correlation of all the data had an average deviation of less than 3 and 93% of the data lies within ±20% (the deviation at a particular data point is defined as the absolute difference between the data and the equation value (Eq. (9)) divided by the data value (Yin et al., 1978)).

Fig. 15 shows the parity plot for the CFD simulations for the range as given in Table 6 (Eq. (10)). The reasoning for the deviation has already been explained in Section 3.1. The parity shows similar deviations for the proposed correlation (Eq. (10)). The comparison with the data of Batchelor (1954) gives a maximum of ±23% deviations. As the AR increases, however, the deviation goes on decreasing. The comparison of the present predictions with the data of Newell and Schmidt (1970) shows a good comparison with deviations in the range of ±4%. A percentage deviation in HTC for the data of Yin et al. (1978) is about ±10%. The data of Lee and Korpela (1983) matches well, with a deviation of ±9%. The data of Zhao et al. (1997) shows a deviation of ±3% while that of Lartigue et al. (2000) shows a deviation of ±6%.

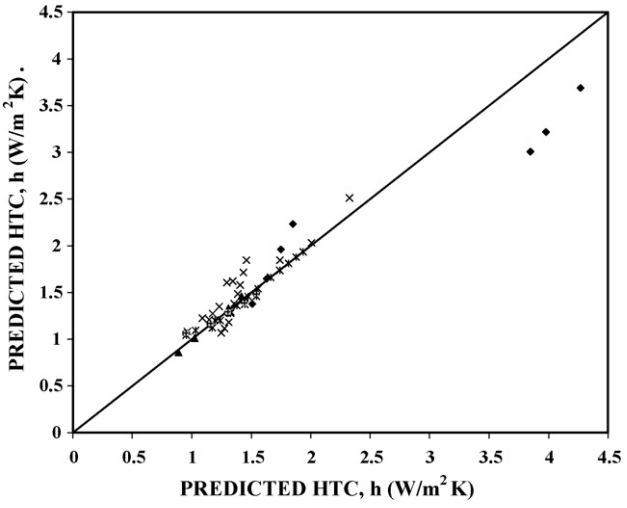

Fig. 15 – Parity plot of predicted heat transfer coefficient for correlation given by Eq. (10): (■) Batchelor (1954); (▲) Newell and Schmidt (1970); (×) Yin et al. (1978); (✱) Lee and Korpela (1983); (✱) Lartigue et al. (2000).

Table 6 – Rayleigh numbers considered for CFD simulations different width and temperature differences.

L (mm)	Temperature difference (ΔT)			
	20	40	60	90
5	5.59E+02	1.12E+03	1.68E+03	2.52E+03
8	2.29E+03	4.58E+03	6.87E+03	1.03E+04
10	4.47E+03	8.95E+03	1.34E+04	2.01E+04
12.5	8.74E+03	1.75E+04	2.62E+04	3.93E+04
15	1.51E+04	3.02E+04	4.53E+04	6.80E+04
20	3.58E+04	7.16E+04	1.07E+05	1.61E+05
25	6.99E+04	1.40E+05	2.10E+05	3.15E+05

4. Conclusions

The following conclusions can be drawn from the present study.

CFD simulations have been performed for specific geometries (Batchelor, 1954; Newell and Schmidt, 1970; Yin et al., 1978; Elsherbiny et al., 1982; Lee and Korpela, 1983) for various heights ($100\,\text{mm} \le H \le 1000\,\text{mm}$), gap widths ($5\,\text{mm} \le L \le 84.7\,\text{mm}$) and temperature differences ($5\,\text{K} \le \Delta T \le 90\,\text{K}$) for tall rectangular vertical enclosures and a good agreement with the literature data and earlier correlations have been obtained (% deviation = ±20%). Further, an effort has been made to list out some of the shortcomings of the earlier literature. CFD simulations over a shorter range of parameters, i.e., $100\,\text{mm} \le H \le 1000\,\text{mm}$; $5\,\text{mm} \le L \le 25\,\text{mm}$ and $20\,\text{K} \le \Delta T \le 90\,\text{K}$ improves the agreement has been obtained (% deviation ±10% except that for the data of Batchelor (1954)).

The two generalized correlations are as follows:

$$Nu = 0.171(Ra)^{0.265}(\text{AR})^{-0.205} \quad 100\,\text{mm} \le H \le 1000\,\text{mm};$$

$$5\,\text{mm} \le L \le 84.7\,\text{mm}; \quad 5\,\text{K} \le \Delta T \le 90\,\text{K}$$

$$Nu = 0.151(Ra)^{0.3}(\text{AR})^{-0.164} \quad 100\,\text{mm} \le H \le 1000\,\text{mm};$$

$$5\,\text{mm} \le L \le 25\,\text{mm}; \quad 20\,\text{K} \le \Delta T \le 90\,\text{K}$$

The effect of flow patterns on the heat transfer coefficient and its importance in predicting the optimum width has been explained comprehensively.

References

Batchelor, G.K., 1954, Heat transfer by free convection across a closed cavity between vertical boundaries at different temperatures. Quart. Appl. Math., 12: 209–233.

Chan, C.L., Yu, Y. and Chen, C.F., 2004, Instability of convection of an ethanol–water solution in a vertical tank. J. Fluid Mech., 510: 243–265.

Eckert, E.G. and Carlson, W.O., 1961, Natural convection in a layer enclosed between two vertical plates with different temperatures. Int. J. Heat Mass Transf., 2: 106–120.

Elder, J.W., 1965, Laminar free convection in a vertical slot. J. Fluid Mech., 23: 77–98.

Elsherbiny, S.M., Raithby, G.D. and Hollands, K.G.T., 1982, Heat transfer by natural convection across vertical and inclined air layers. Trans. ASME J. Heat Transf., 104: 96–102.

FLUENT 6.2., 2005. User's Manual to FLUENT 6.2. Fluent, Inc. Centrera Resource Park, 10 Cavendish Court, Lebanon, USA.

Ganguli, A.A., Pandit, A.B. and Joshi, J.B., 2007, Numerical predictions of flow patterns due to natural convection in a vertical slot. Chem. Eng. Sci., 62(16): 4479–4495.

Incropera, F.P. and Dewitt, D.P., (2002). *Fundamentals of Heat and Mass Transfer* (5th ed.). (Wiley & Sons, New York) (Appendix-A, p. 917)

Jakob, M., (1949). *Heat Transfer* (Wiley & Sons, New York) (Chapter 25)

Korpela, S., Lee, Y. and Drummond, J.E., 1982, Heat transfer through a double pane window. Trans. ASME J. Heat Transf., 104: 539–544.

Lartigue, B., Lorente, S. and Bourret, B., 2000, Multicellular natural convection in high aspect ratio cavity: experimental and numerical results. Int. J. Heat Mass Transf., 43: 3157–3170.

Le Quéré, P., 1990, A note on multiple and unsteady solutions in two-dimensional convection in a tall cavity. Trans. ASME J. Heat Transf., 112: 965–973.

Lee, Y. and Korpela, S., 1983, Multicellular natural convection in a vertical slot. J. Fluid Mech., 126: 91–124.

Newell, M.E. and Schmidt, F.W., 1970, Heat transfer by laminar natural convection within rectangular enclosures. Trans. ASME C: J. Heat Transf., 92: 159–167.

Wakitani, S., 1994, Experiments on convective instability of large Prandtl number fluids in a vertical slot. J. Fluid Mech., 116: 120–126.

Wakitani, S., 1996, Formation of cells in natural convection in a vertical slot at large Prandtl number. J. Fluid Mech., 314: 299–314.

Wakitani, S., 1997, Development of multicellular solutions in natural convection in an air-filled vertical cavity. Trans. ASME J. Heat Transf., 119: 97–101.

Yin, S.H., Wung, T.Y. and Chen, K., 1978, Natural convection in an air layer enclosed within rectangular cavities. Int. Heat Mass Transf., 21: 307–315.

Zhao, Y., Curcija, D. and Gross, W.P., 1997, Prediction of multicellular flow regime of natural convection in fenestration glazing cavities. ASHRAE Trans., 103(1): 1–12.